

ON THE TRUE-AMPLITUDE IMAGING CONDITION FOR REVERSE-TIME MIGRATION

N. Albano, J. C. Costa, J. Schleicher, and A. Novais

email: *js@ime.unicamp.br*

keywords: *Reverse-time migration, Imaging condition, True amplitude*

ABSTRACT

The true-amplitude (TA) imaging condition for reverse-time migration (RTM) is based on a combination of temporal and spatial derivatives of the up- and downgoing wavefields. By means of partial integrations (or redistribution of the frequency factors in the frequency domain, we derive several alternative expressions for this imaging condition. Interestingly, the temporal derivatives can be completely replaced by spatial derivatives and temporal integrations. In this way, one version of the TA imaging condition makes use of the Laplacian operator, in this way relating to a common way of removing backscattering artifacts in RTM. We demonstrate by means of numerical examples using the Marmousi and Sigsbee2A data that the quality of the migrated image strongly depends on the version chosen for implementation. The best quality is achieved with a version that combines second derivatives of the source wavefield with the Laplacian operator.

INTRODUCTION

Reverse-time migration (RTM) is a seismic imaging method based on the full (two-way) wave equation (Schultz and Sherwood, 1980; McMechan, 1983; Baysal et al., 1983; Sun and McMechan, 2001; Yan and Sava, 2008). In the same way as other wave-equation based migration techniques, it makes use of an image condition, the most basic form of which is simple cross-correlation of the up- and downgoing wavefields (Claerbout, 1971).

In the early days of seismic imaging, RTM was not of much practical use because of its high computational cost and the presence of strong low-frequency artifacts from backscattering if the velocity model contains sharp velocity contrasts. Its use has gained much popularity in the first decade of this century, after the advent of more powerful computers and new technologies to remove the backscattering artifacts (Yoon et al., 2004; Fletcher et al., 2006; Guitton et al., 2006). Most of these techniques rely on modified imaging conditions (see, e.g., Yoon and Marfurt, 2006; Costa et al., 2009; Luo et al., 2009, 2010; Zhu et al., 2009). In the same context, Kiyashchenko et al. (2007) and Op't Root et al. (2012) derive the true-amplitude (TA) imaging condition for reverse-time migration (RTM). The purpose of the TA imaging condition is to remove the backscattering artifacts and to provide image amplitudes that are proportional to reflection coefficients.

Unfortunately, in the form presented by these authors, the TA imaging condition does not allow for an efficient implementation in the time domain. For a time-domain implementation, it must be recast into a different form. In this paper, we derive a number of theoretically equivalent forms of the approximate TA imaging condition that can be efficiently implemented in the time domain. In a similar way to Douma et al. (2010), we show that the true-amplitude imaging condition for RTM can be reformulated into a version containing the Laplacian operator. This operator is frequently used in seismic imaging without a profound theoretical basis to remove the low-frequency backscattering artifacts from RTM images. We numerically evaluate the derived time-domain versions of the TA imaging condition by comparing the resulting migrated images of the Marmousi and Sigsbee2A data.

TRUE-AMPLITUDE IMAGING CONDITION

According to Op't Root et al. (2012), the TA imaging condition is given in the frequency domain by

$$I_r(\mathbf{x}) = \frac{1}{2\pi} \sum_s \int_{\omega} d\omega \frac{1}{(-i\omega)P_s\bar{P}_s} \left[\bar{P}_s P_r - \frac{c^2(\mathbf{x})}{\omega^2} \nabla \bar{P}_s \cdot \nabla P_r \right], \quad (1)$$

where $P_s = P_s(\omega, \mathbf{x}; \mathbf{x}_s)$ and $P_r = P_r(\omega, \mathbf{x}; \mathbf{x}_s)$ are the (downgoing) source and (upgoing) receiver wavefields for a source at \mathbf{x}_s , downward continued to the imaging point \mathbf{x} . Moreover, the bar over a symbol denotes the complex conjugate operation.

Equation (1) is slightly different from the one of Op't Root et al. (2012). For simplicity, we have assumed that the source wavelet is a (possibly band-limited) delta-function, the effects of which are acceptable in the final migrated image. Therefore, we have combined in equation (1) the Green's function and source wavelet in the formula of Op't Root et al. (2012) into the source wavefield P_s . Moreover, we have made the sum over all sources explicit. Finally, the different sign of the factor $(-i\omega)$ in the denominator of the above equation results from our use of the following definition of the Fourier transform pair,

$$f(\omega) = \int_{-\infty}^{\infty} dt f(t) e^{i\omega t} \quad \text{e} \quad f(t) = \frac{1}{2\pi} \int_{-\infty}^{\infty} d\omega f(\omega) e^{-i\omega t}. \quad (2)$$

When trying to implement the TA imaging condition in the time domain, one recognizes that its basic form, equation (1) is not very favorable. For an efficient time-domain implementation, it must be recast into a more adequate form. Below, we derive a number of theoretically equivalent forms. We then compare them numerically by looking at the corresponding images.

Implementational forms

The advantage of the frequency domain representation of the TA imaging condition in equation (1) is that the time derivatives are represented by factors $(-i\omega)$. Thus, it immediately allows us to recognize that these factors can be rather freely redistributed among the wavefield terms. Making use of this freedom, our first rewrite moves the ω^2 in the denominator of the spatial-derivatives term, where it would represent a two-fold time integration, to a position in front of the parentheses. This results in

$$\begin{aligned} I_r(\mathbf{x}) &= \sum_s \int_{\omega} d\omega \frac{1}{(-i\omega)(-\omega^2)P_s\bar{P}_s} \left[-\omega^2 \bar{P}_s P_r + c^2(\mathbf{x}) \nabla \bar{P}_s \cdot \nabla P_r \right], \\ &= \sum_s \int_{\omega} d\omega \frac{1}{(-i\omega)^3 P_s \bar{P}_s} \left[(-i\omega) \bar{P}_s (-i\omega) P_r + c^2(\mathbf{x}) \nabla \bar{P}_s \cdot \nabla P_r \right], \end{aligned} \quad (3)$$

where the second equation results from distributing the $(-i\omega)$ factors symmetrically between the wavefield terms. This is the most conventional form of applying the time derivatives.

If we move one of the $(-i\omega)$ factors in the denominator to the receiver wavefield, we can rewrite equation (3) as

$$I_r(\mathbf{x}) = \sum_s \int_{\omega} d\omega \frac{1}{(-i\omega)^2 P_s \bar{P}_s} \left[(-i\omega) \bar{P}_s (-i\omega) Q_r + c^2(\mathbf{x}) \nabla \bar{P}_s \cdot \nabla Q_r \right], \quad (4)$$

where we have introduced the integrated receiver wavefield

$$q_r(t, \mathbf{x}; \mathbf{x}_s) = \int_0^t p_r(t', \mathbf{x}; \mathbf{x}_s) dt' \quad \text{i.e.,} \quad Q_r = Q_r(\omega, \mathbf{x}; \mathbf{x}_s) = \frac{P_r(\omega, \mathbf{x}; \mathbf{x}_s)}{(-i\omega)}. \quad (5)$$

Under the assumption that the absolute value of the source wavefield is locally frequency independent, which is consistent with the approximation $P_s(\omega, \mathbf{x}; \mathbf{x}_s) = A_s(\mathbf{x}; \mathbf{x}_s) e^{-i\omega \tau_s(\mathbf{x}; \mathbf{x}_s)}$, the illumination-compensation factor in the denominator can be taken out of the frequency integral (see also Kiyashchenko et al., 2007; Schleicher et al., 2008). In this way, equation (4) can be approximated by

$$I_r(\mathbf{x}) = \sum_s \frac{1}{P'(\mathbf{x}; \mathbf{x}_s)} \int_{\omega} d\omega \left[(-i\omega) \bar{P}_s (-i\omega) Q_r + c^2(\mathbf{x}) \nabla \bar{P}_s \cdot \nabla Q_r \right], \quad (6)$$

or in the time domain,

$$I_r(\mathbf{x}) = \sum_s \frac{1}{P'(\mathbf{x}, \mathbf{x}_s)} \int_t dt [\dot{p}_s(t, \mathbf{x}; \mathbf{x}_s) \dot{q}_r(t, \mathbf{x}; \mathbf{x}_s) + c^2(\mathbf{x}) \nabla p_s(t, \mathbf{x}; \mathbf{x}_s) \cdot \nabla q_r(t, \mathbf{x}; \mathbf{x}_s)] , \quad (7)$$

where the dot above a symbol denotes the time derivative. The illumination compensation factor $P'(\mathbf{x}, \mathbf{x}_s)$ is given by the autocorrelation of the time derivative of the source wavefield, i.e.,

$$P'(\mathbf{x}; \mathbf{x}_s) = \int_\omega d\omega (-i\omega P_s)(-i\omega) \overline{P_s} = \int_t dt (\dot{p}_s(t, \mathbf{x}; \mathbf{x}_s))^2 . \quad (8)$$

When the TA imaging condition is to be implemented in the form of equation (7), we need to propagate the source wavefield and the time integral of the receiver wavefield. Of both these wavefields, we need to take the temporal and spatial derivatives at the image point before correlation, summation and illumination compensation.

If we want to avoid calculation of the time derivative of the source wavefield, we can use the third time integral of the receiver wavefield instead. Introducing

$$q_r^{(3)} = \int_0^t q_r^{(2)}(t') dt' \text{ with } q_r^{(2)} = \int_0^t q_r(t') dt', \quad \text{i.e.,} \quad Q_r^{(3)} = \frac{P_r}{(-i\omega)^3} = -\frac{Q_r}{\omega^2} , \quad (9)$$

we can rewrite equation (4) as

$$I_r(\mathbf{x}) = \sum_s \frac{1}{P(\mathbf{x}; \mathbf{x}_s)} \int_\omega d\omega [(-i\omega) \overline{P_s} (-i\omega) Q_r^{(3)} + c^2(\mathbf{x}) \nabla \overline{P_s} \cdot \nabla Q_r^{(3)}] , \quad (10)$$

or in the time domain,

$$I_r(\mathbf{x}) = \sum_s \frac{1}{P(\mathbf{x}, \mathbf{x}_s)} \int_t dt [\dot{p}_s(t, \mathbf{x}; \mathbf{x}_s) \dot{q}_r^{(3)}(t, \mathbf{x}; \mathbf{x}_s) + c^2(\mathbf{x}) \nabla p_s(t, \mathbf{x}; \mathbf{x}_s) \cdot \nabla q_r^{(3)}(t, \mathbf{x}; \mathbf{x}_s)] . \quad (11)$$

In this version of the TA imaging condition, the illumination factor $P(\mathbf{x}; \mathbf{x}_s)$ is given by the autocorrelation of the source wavefield, i.e.,

$$P(\mathbf{x}, \mathbf{x}_s) = \int_\omega d\omega P_s(\omega, \mathbf{x}; \mathbf{x}_s) \overline{P_s}(\omega, \mathbf{x}; \mathbf{x}_s) = \int_t dt (p_s(t, \mathbf{x}; \mathbf{x}_s))^2 . \quad (12)$$

In equation (10), we again have made use of the local frequency independence of the absolute value of the source wavefield, which allows us to take the illumination compensation factor out of the frequency integral. We will consistently keep doing this for all remaining versions of the TA imaging condition.

For the application of the TA imaging condition in the form of equation (11), we need to propagate the source wavefield and the triple time-integrated receiver wavefield. We need to calculate the temporal and spatial derivatives of these wavefields before correlation and summation, but not for the illumination compensation.

Another alternative form of the TA imaging condition is obtained when using the second time derivative of the source wavefield given by

$$r_s = \ddot{p}_s \quad \text{i.e.,} \quad R_s = -\omega^2 P_s . \quad (13)$$

Adequate distribution of the $(i\omega)$ factors in equation (4) leads to the expression

$$I_r(\mathbf{x}) = \sum_s \int_\omega d\omega \frac{1}{R_s \overline{R_s}} [(-i\omega) \overline{R_s} (-i\omega) Q_r + c^2(\mathbf{x}) \nabla \overline{R_s} \cdot \nabla Q_r] . \quad (14)$$

Again taking the illumination compensation out of the frequency integral, we arrive at

$$I_r(\mathbf{x}) = \sum_s \frac{1}{R(\mathbf{x}; \mathbf{x}_s)} \int_\omega d\omega [(-i\omega) \overline{R_s} (-i\omega) Q_r + c^2(\mathbf{x}) \nabla \overline{R_s} \cdot \nabla Q_r] , \quad (15)$$

or in the time domain,

$$I_r(\mathbf{x}) = \sum_s \frac{1}{R(\mathbf{x}, \mathbf{x}_s)} \int_t dt [\dot{r}_s(t, \mathbf{x}; \mathbf{x}_s) \dot{q}_r(t, \mathbf{x}; \mathbf{x}_s) + c^2(\mathbf{x}) \nabla r_s(t, \mathbf{x}; \mathbf{x}_s) \cdot \nabla q_r(t, \mathbf{x}; \mathbf{x}_s)] . \quad (16)$$

In this version of the TA imaging condition, the illumination compensation factor $R(\mathbf{x}, \mathbf{x}_s)$ is given by the autocorrelation of the second time derivative of the source field, i.e.,

$$R(\mathbf{x}, \mathbf{x}_s) = \int_\omega d\omega R_s(\omega, \mathbf{x}; \mathbf{x}_s) \overline{R_s(\omega, \mathbf{x}; \mathbf{x}_s)} = \int_t dt (r_s(t, \mathbf{x}; \mathbf{x}_s))^2 . \quad (17)$$

For the application of the TA imaging condition in the form of equation (16), we need to propagate the second time derivative of the source wavefield and the time integral of the receiver wavefields. We then need to calculate the temporal and spatial derivatives for the correlation and sum, but not for the illumination compensation.

RELATIONSHIP WITH THE LAPLACIAN

It is not hard to conceive that the redistribution of the $(-i\omega)$ factors in equation (4) needs not be done symmetrically with respect to the involved wavefields. Instead of applying one factor to the source wavefield and the second one to the receiver wavefields, we can apply both factors to only one of these wavefields, say, the source wavefield. For convenience, we also move the velocity square to obtain

$$I_r(\mathbf{x}) = \sum_s \int_\omega d\omega \frac{c^2(\mathbf{x})}{P_s \overline{P_s}} \left[-\frac{\omega^2}{c^2(\mathbf{x})} \overline{P_s} Q_r^{(3)} + \nabla \overline{P_s} \cdot \nabla Q_r^{(3)} \right] . \quad (18)$$

On the one hand, the factor ω^2/c^2 can be interpreted as multiplying the source wavefield. Upon the use of the corresponding Helmholtz equation,

$$\nabla^2 P_s + \frac{\omega^2}{c^2(\mathbf{x})} P_s = 0 , \quad (19)$$

equation (18) becomes

$$\begin{aligned} I_r(\mathbf{x}) &= \sum_s \int_\omega d\omega \frac{c^2(\mathbf{x})}{P_s \overline{P_s}} \left[\nabla^2 \overline{P_s} Q_r^{(3)} + \nabla \overline{P_s} \cdot \nabla Q_r^{(3)} \right] \\ &= \sum_s \int_\omega d\omega \frac{c^2(\mathbf{x})}{P_s \overline{P_s}} \nabla \cdot \left[\nabla \overline{P_s} Q_r^{(3)} \right] , \end{aligned} \quad (20)$$

where the second equality is a result of recognizing the product rule for the spatial derivatives. Taking the illumination compensation out of the frequency integral, we can rewrite equation (20) as

$$I_r(\mathbf{x}) = \sum_s \frac{c^2(\mathbf{x})}{P(\mathbf{x}; \mathbf{x}_s)} \int_\omega d\omega \nabla \cdot \left[\nabla \overline{P_s} Q_r^{(3)} \right] , \quad (21)$$

where $P(\mathbf{x}; \mathbf{x}_s)$ is given by equation (12).

On the other hand, we can also interpret the factor ω^2/c^2 as multiplying the receiver wavefield. Using the (third time integral of the) associated Helmholtz equation,

$$\nabla^2 Q_r^{(3)} + \frac{\omega^2}{c^2(\mathbf{x})} Q_r^{(3)} = 0 , \quad (22)$$

we can rewrite equation (18) as

$$\begin{aligned} I_r(\mathbf{x}) &= \sum_s \int_\omega d\omega \frac{c^2(\mathbf{x})}{P_s \overline{P_s}} \left[\overline{P_s} \nabla^2 Q_r^{(3)} + \nabla \overline{P_s} \cdot \nabla Q_r^{(3)} \right] \\ &= \sum_s \int_\omega d\omega \frac{c^2(\mathbf{x})}{P_s \overline{P_s}} \nabla \left[\overline{P_s} \nabla Q_r^{(3)} \right] , \end{aligned} \quad (23)$$

or

$$I_r(\mathbf{x}) = \sum_s \frac{c^2(\mathbf{x})}{P(\mathbf{x}; \mathbf{x}_s)} \int_{\omega} d\omega \nabla \left[\overline{P_s} \nabla Q_r^{(3)} \right], \quad (24)$$

Moreover, since equations (20) and (23) represent manipulations of the same theoretical expression (4), we can also calculate the image I_r as the average of both expressions, i.e.,

$$\begin{aligned} I_r(\mathbf{x}) &= \sum_s \int_{\omega} d\omega \frac{c^2(\mathbf{x})}{P_s \overline{P_s}} \frac{1}{2} \left(\nabla \cdot \left[\nabla \overline{P_s} Q_r^{(3)} \right] + \nabla \cdot \left[\overline{P_s} \nabla Q_r^{(3)} \right] \right) \\ &= \sum_s \int_{\omega} d\omega \frac{c^2(\mathbf{x})}{2P_s \overline{P_s}} \left(\nabla \cdot \left[\nabla \overline{P_s} Q_r^{(3)} + \overline{P_s} \nabla Q_r^{(3)} \right] \right) \\ &= \sum_s \int_{\omega} d\omega \frac{c^2(\mathbf{x})}{2P_s \overline{P_s}} \nabla^2 \left[\overline{P_s} Q_r^{(3)} \right], \end{aligned} \quad (25)$$

where we again have made use of the product rule for the gradient.

Taking the illumination compensation together with the Laplacian out of the frequency integral, we arrive at

$$I_r(\mathbf{x}) = \sum_s \frac{c^2(\mathbf{x})}{2P(\mathbf{x}; \mathbf{x}_s)} \nabla^2 \int_{\omega} d\omega \left[\overline{P_s} Q_r^{(3)} \right], \quad (26)$$

or in the time domain,

$$I_r(\mathbf{x}) = \sum_s \frac{c^2(\mathbf{x})}{2P(\mathbf{x}; \mathbf{x}_s)} \nabla^2 \int_t dt \left[p_s(t, \mathbf{x}; \mathbf{x}_s) q_r^{(3)}(t, \mathbf{x}; \mathbf{x}_s) \right], \quad (27)$$

where $P(\mathbf{x}; \mathbf{x}_s)$ is again given by equation (12).

We note that, except for a small modification, the TA imaging condition in this form is equivalent of the application of the Laplacian to the correlation of the source and receiver wavefields, which is a common procedure in practice. The small modification is the use of the third time integral of the receiver wavefield and a multiplication with a factor of $c^2/2$.

Of course, the same manipulations can be applied to the form (14) of the TA imaging condition, resulting in

$$I_r(\mathbf{x}) = \sum_s \frac{c^2(\mathbf{x})}{2R(\mathbf{x}; \mathbf{x}_s)} \nabla^2 \int_{\omega} d\omega \left[\overline{R_s} Q_r \right], \quad (28)$$

or in the time domain,

$$I_r(\mathbf{x}) = \sum_s \frac{c^2(\mathbf{x})}{2R(\mathbf{x}; \mathbf{x}_s)} \nabla^2 \int_t dt \left[r_s(t, \mathbf{x}; \mathbf{x}_s) q_r(t, \mathbf{x}; \mathbf{x}_s) \right], \quad (29)$$

where $R(\mathbf{x}; \mathbf{x}_s)$ is given by equação (17).

NUMERICAL EXAMPLES

We have implemented the above discussed versions of the TA imaging condition and applied them in a reverse-time migration of the Marmousi data. All migrations used the same algorithm for propagation of the involved wavefields in a smoothed version of the Marmousi model (see Figure 1. A set of reference images, Figures 2 to 5 show the result of RTM using the conventional crosscorrelation imaging condition of Claerbout (1971) without further post-processing, with illumination compensation through division by the autocorrelation of the source wavefield, with Laplacian filtering, and with both illumination compensation and Laplacian filtering.

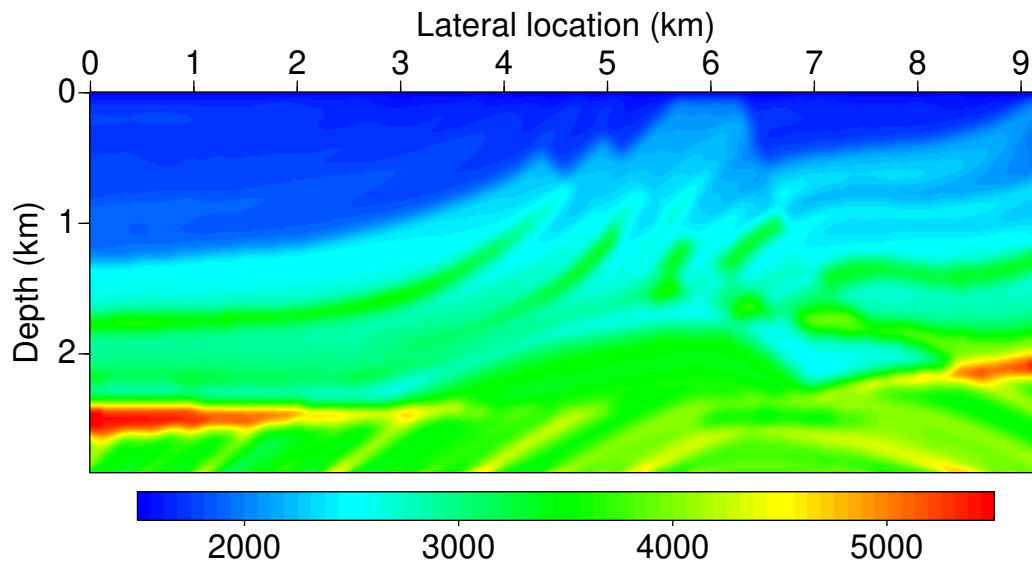


Figure 1: Smoothed Marmousi model used for reverse-time migration for the application of the different imaging conditions.

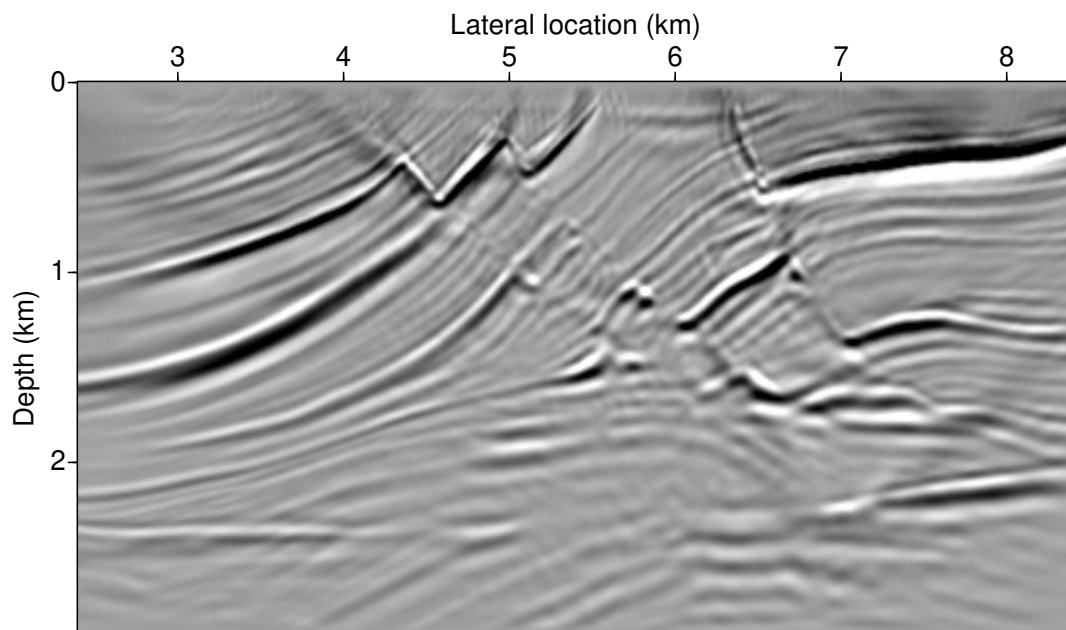


Figure 2: RTM of the Marmousi data using the conventional crosscorrelation imaging condition.

Figure 2 shows that the simple crosscorrelation imaging condition alone leads to strong backscattering artifacts and decreasing amplitudes with depth. In this way, only the strongest reflectors are visible in the image. The amplitude loss with depth is corrected for by the illumination compensation (see Figure 3), and the backscattering is removed by the Laplacian filter (see Figure 4). Both post-processing filters together produce the rather clean image of Figure 5.

Figure 6 depicts the result of RTM using the TA imaging condition in the version of equation (7). We observe that in addition to cleaning the image in a similar way to the post-processing filters in Figure 5,

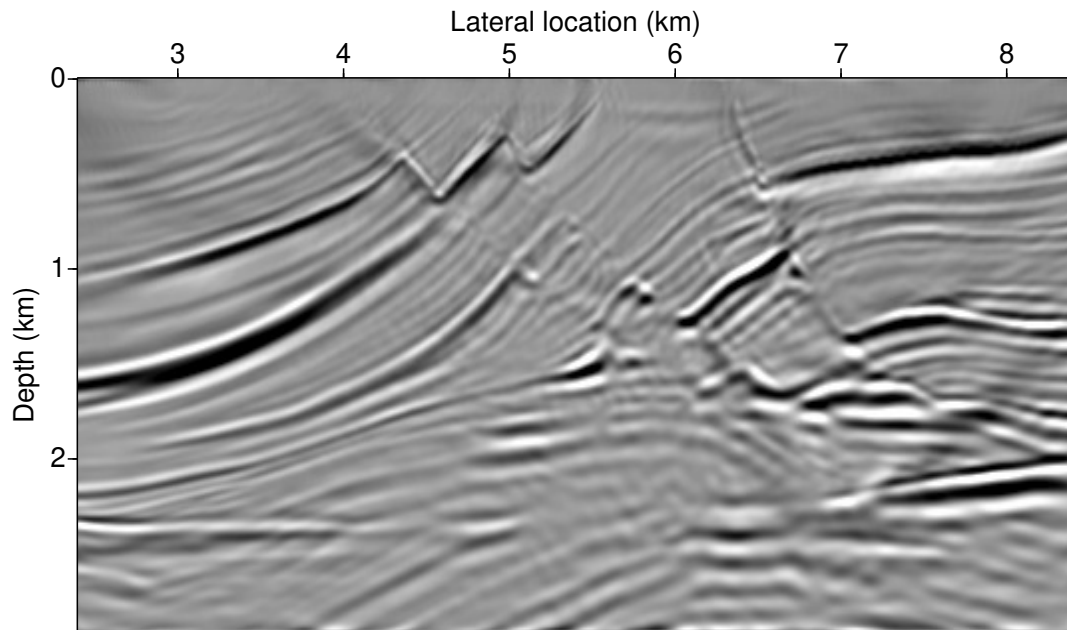


Figure 3: RTM of the Marmousi data using the conventional crosscorrelation imaging condition with illumination compensation.

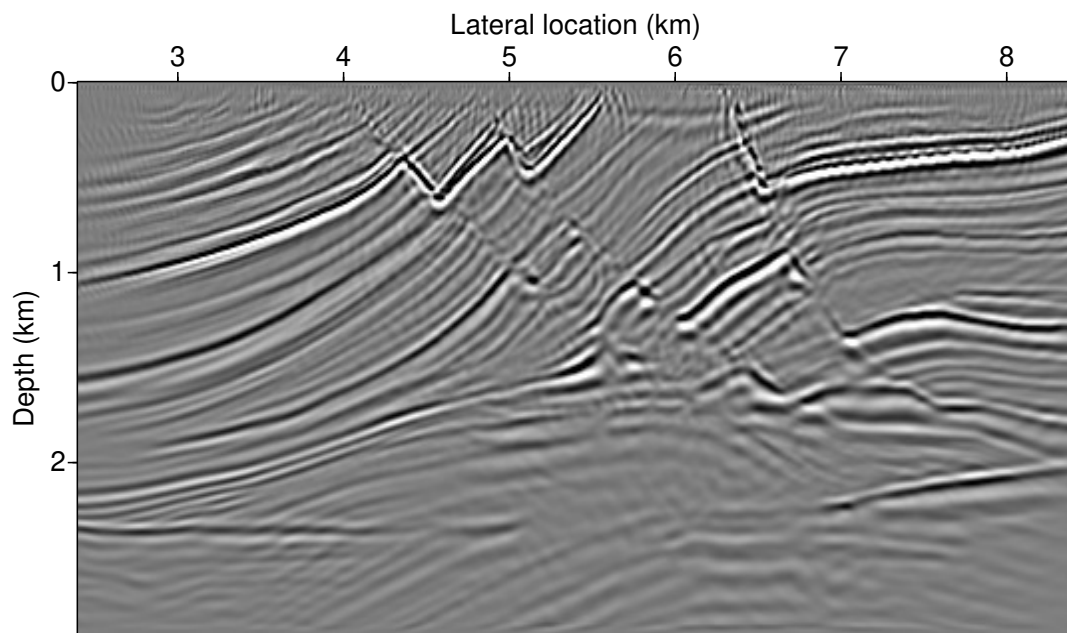


Figure 4: RTM of the Marmousi data using the conventional crosscorrelation imaging condition with Laplacian filtering.

the TA imaging condition leads to a better preservation of relative amplitudes. Particularly in the deeper portion of the image, the reflectors are better visible. However, as we will see below, this is still not the best image that can be obtained with the TA imaging condition.

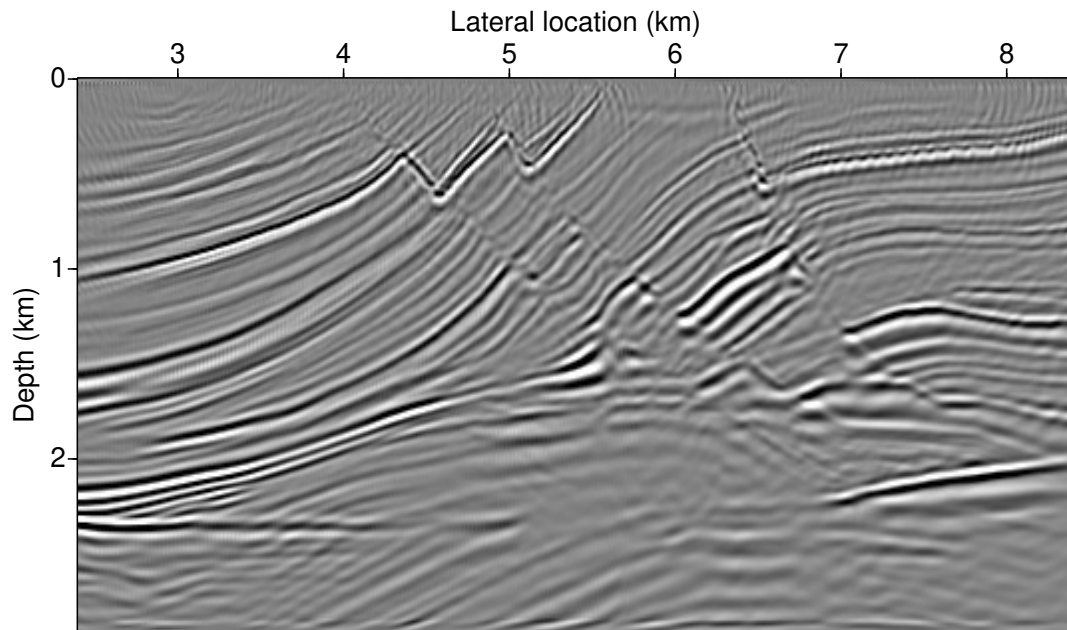


Figure 5: RTM of the Marmousi data using the conventional crosscorrelation imaging condition with illumination compensation and Laplacian filtering.

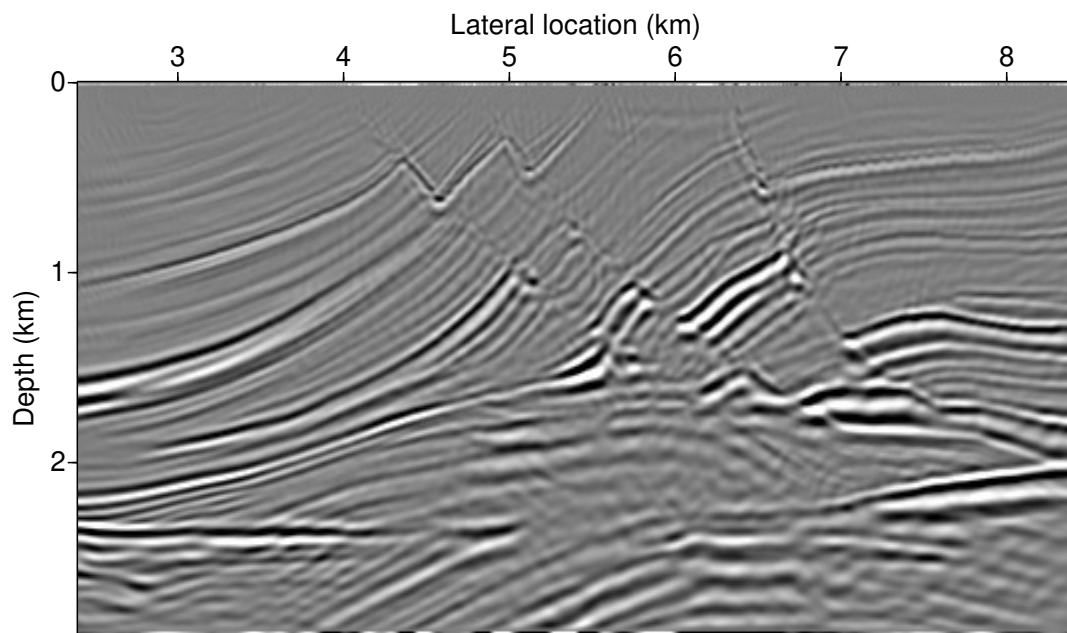


Figure 6: RTM of the Marmousi data using the TA imaging condition in the version of equation (7).

Figure 7 shows the result of RTM using the version of equation (11). This figure demonstrates that this version of the TA imaging condition is rather unstable, particularly at shallow depth. Also, resolution is somewhat lower. Probably, the reason for these effects is the involved third time integral of the receiver wavefield, which enhances low frequencies and can create artifacts at the beginning and end of a seismic

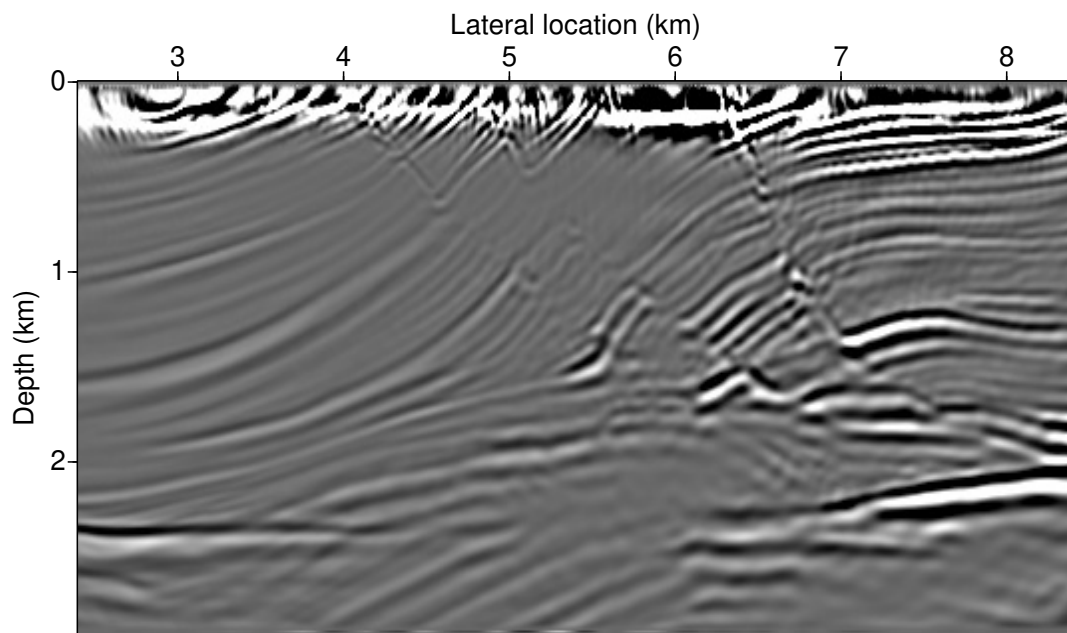


Figure 7: RTM of the Marmousi data using the TA imaging condition in the version of equation (11).

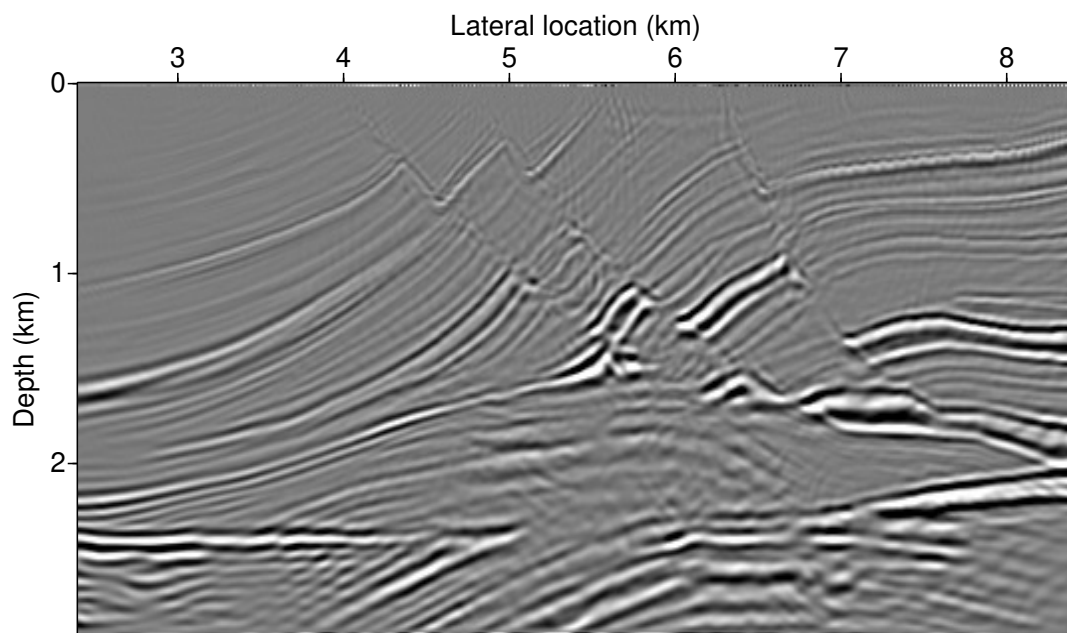


Figure 8: RTM of the Marmousi data using the TA imaging condition in the version of equation (16).

trace. Further research is required to stabilize the numerical realization of the triple integration.

Figure 8 shows the result of RTM using the version of equation (16). This figure demonstrates that use of this version, which uses second derivatives of the source wavefield both in the correlation part and the illumination compensation, helps to produce a very clean image that even presents slightly improved resolution over the basic version of equation (11) in Figure 6.

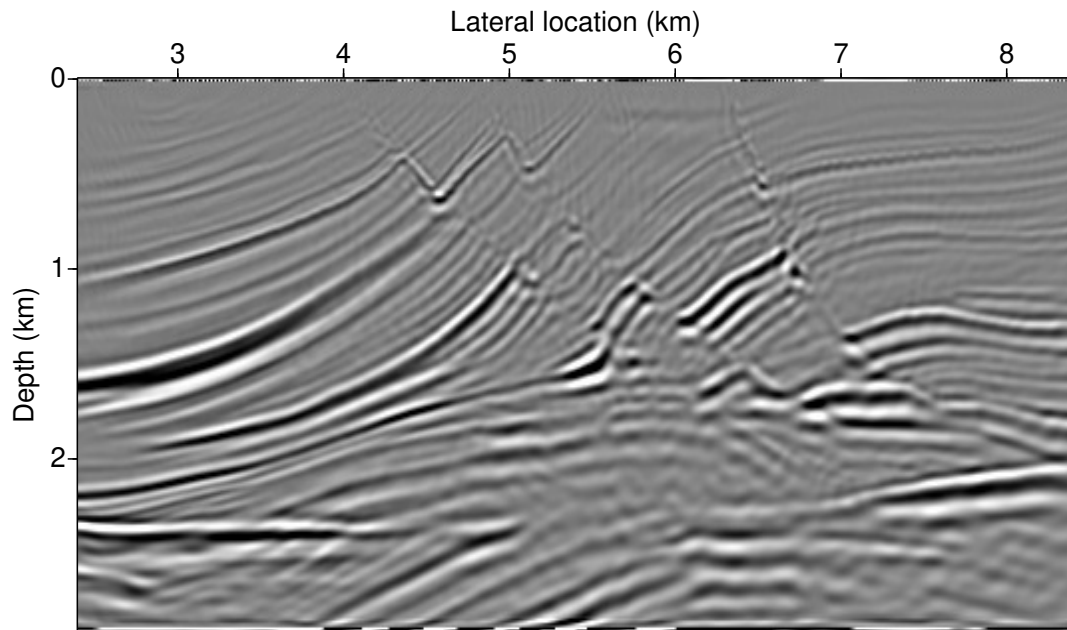


Figure 9: RTM of the Marmousi data using the TA imaging condition in the version of equation (27).

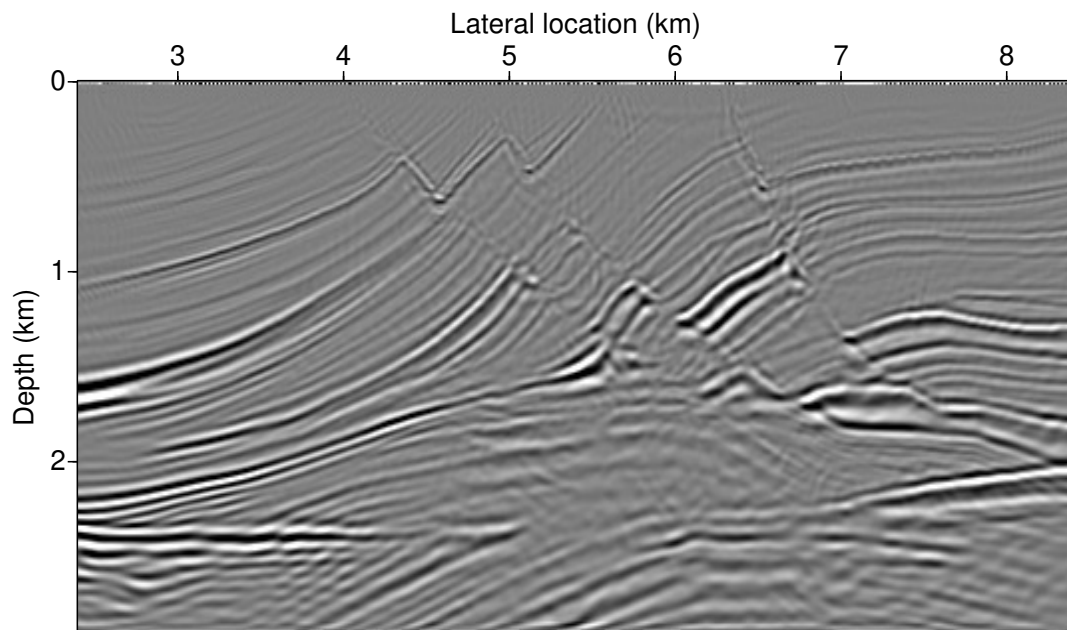


Figure 10: RTM of the Marmousi data using the TA imaging condition in the version of equation (29).

In contrast, the image obtained with version (27) of the TA imaging condition involving the thrice time-integrated receiver wavefield and the Laplacian filter (see Figure 9), slightly decreases the resolution as compared to the image of Figure 6. While the quality does not degrade to the same degree as in Figure 7, apparently also in this version the triple integration of the receiver wavefield is enhancing the low frequencies too much.

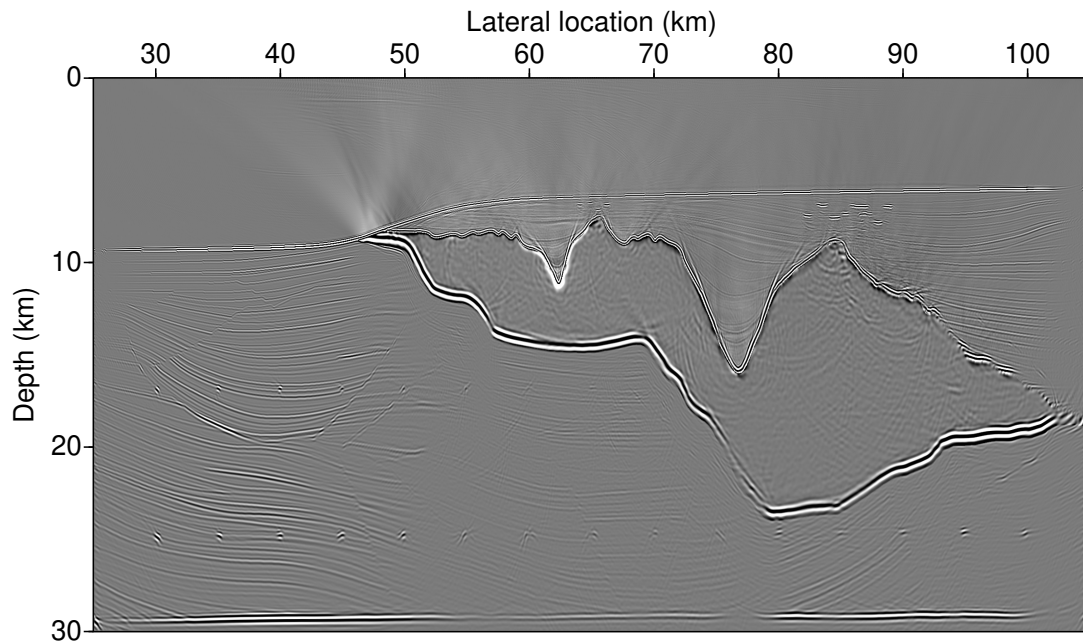


Figure 11: RTM of the Sigsbee2A data using the TA imaging condition in the version of equation (7).

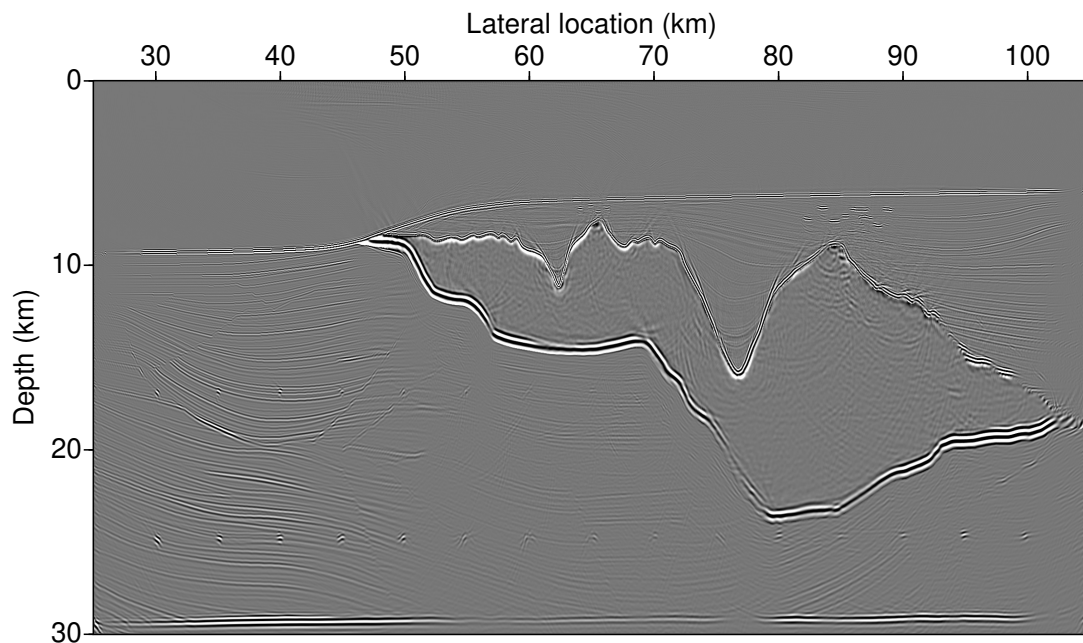


Figure 12: RTM of the Sigsbee2A data using the TA imaging condition in the version of equation (29).

Finally, Figure 10 shows the image obtained with version (29) of the TA imaging condition, involving the second derivatives of the source wavefield and the Laplacian filter. As we can see, this image is the best one obtained with all our versions of the TA imaging condition. The resolution is further enhanced as compared with Figure 8. Relative reflector amplitudes nicely correspond to relative reflectivity changes. In this way, many weak reflectors of the Marmousi model can be clearly delineated.

To corroborate our findings, we have applied the basic version of the TA imaging condition, equation (7), and the one that yielded the best results on the Marmousi data, equation (29), to the Sigsbee2A data set. Figures 11 and 12 show the results. We see that for this data set the former version of the TA imaging condition retains some backscattering noise in the image, whereas the latter version is much cleaner and also improves the resolution. Again, relative reflector amplitudes nicely resemble reflectivities.

CONCLUSIONS

In this paper, we have implemented a number of theoretically equivalent versions of the true-amplitude imaging condition for RTM of Kiyashchenko et al. (2007) and Op't Root et al. (2012). In a similar way to Douma et al. (2010), our theoretical derivations have show a relationship between the true-amplitude imaging condition for RTM and the Laplacian operator. This operator is frequently used in seismic imaging without a profound theoretical basis to remove low-frequency backscattering artifacts from RTM images. By means of our numerical tests on the Marmousi and Sigsbee2A data sets, we have seen that the actual implementational form matters and may lead to significantly different image quality. We have shown that all our implementational forms of the TA imaging condition provide superior results that simple cross-correlation of the source and receiver wavefields, even if illumination compensation and Laplacian filtering are applied. The Laplacian-based formulation of the TA imaging condition using the second derivatives of the source wavefield is the one that provided the best image quality, leading to the best suppression of backscattering artifacts and the highest image resolution.

ACKNOWLEDGMENTS

This work was kindly supported by CNPq, CAPES, and the sponsors of the *Wave Inversion Technology (WIT) Consortium*.

REFERENCES

- Baysal, E., Kosloff, D., and Sherwood, W. (1983). Reverse time migration. *Geophysics*, 48(11):1514–1524.
- Claerbout, J. F. (1971). Toward a unified theory of reflector mapping. *Geophysics*, 36(3):467–481.
- Costa, J. C., Neto, F. A. S., Alcântara, M. R. M., Schleicher, J., and Novais, A. (2009). Obliquity-correction imaging condition for reverse time migration. *Geophysics*, 74(3):S57–S66.
- Douma, H., Yingst, D., Vasconcelos, I., and Tromp, J. (2010). On the connection between artifact filtering in reverse-time migration and adjoint tomography. *GEOPHYSICS*, 75(6):S219–S223.
- Fletcher, R. P., Fowler, P. J., Kitchenside, P., and Albertin, U. (2006). Suppressing unwanted internal reflections in prestack reverse-time migration. *Geophysics*, 71(6):E79–E82.
- Guitton, A., Kaelin, B., and Biondi, B. (2006). Least-squares attenuation of reverse time migration artifacts. In *SEG Technical Program Expanded Abstracts*, pages 2348–2352.
- Kiyashchenko, D., Plessix, R.-E., Kashtan, B., and Troyan, V. (2007). A modified imaging principle for true-amplitude wave-equation migration. *Geophysical Journal International*, 168(3):1093–1104.
- Luo, Y., Zhu, H., Nissen-Meyer, T., Morency, C., Peter, D., and Tromp, J. (2010). Modeling and imaging based upon spectral-element and adjoint methods. In *SEG Technical Program Expanded Abstracts 2010*. Society of Exploration Geophysicists.
- Luo, Y., Zhu, H., Nissen-Meyer, T., Morency, C., and Tromp, J. (2009). Seismic modeling and imaging based upon spectral-element and adjoint methods. *The Leading Edge*, 28(5):568–574.
- McMechan, G. A. (1983). Migration by extrapolation of time-dependent boundary values. *Geophysical Prospecting*, 31(3):413–420.
- Op't Root, T. J., Stolk, C. C., and Maarten, V. (2012). Linearized inverse scattering based on seismic reverse time migration. *Journal de mathématiques pures et appliquées*, 98(2):211–238.

- Schleicher, J., Costa, J. C., and Novais, A. (2008). Time-migration velocity analysis by image-wave propagation of common-image gathers. *Geophysics*, 73(5):VE161–VE171.
- Schultz, P. S. and Sherwood, J. W. C. (1980). Depth migration before stack. *Geophysics*, 45(3):376–393.
- Sun, R. and McMechan, G. A. (2001). Scalar reverse-time depth migration of prestack elastic seismic data. *GEOPHYSICS*, 66(5):1519–1527.
- Yan, J. and Sava, P. (2008). Isotropic angle-domain elastic reverse-time migration. *GEOPHYSICS*, 73(6):S229–S239.
- Yoon, K. and Marfurt, K. (2006). Reverse-time migration using the Poynting vector. *Exploration Geophysics*, 37:102–107.
- Yoon, K., Marfurt, K. J., and Starr, W. (2004). Challenges in reverse-time migration. In *SEG Technical Program Expanded Abstracts 2004*. Society of Exploration Geophysicists.
- Zhu, H., Luo, Y., Nissen-Meyer, T., Morency, C., and Tromp, J. (2009). Elastic imaging and time-lapse migration based on adjoint methods. *GEOPHYSICS*, 74(6):WCA167–WCA177.